Cell Adhesion-Dependent Biphasic Axon Outgrowth Elucidated by Femtosecond Laser Impulse

Sohei Yamada[a,b,*], Kentarou Baba[c], Naoyuki Inagaki[c], Yoichiroh Hosokawa[a,*]

[a] Division of Materials Science, Nara Institute of Science and Technology, 8916-5 Takayama, Ikoma, Nara 630-0192, Japan

[b] Graduate School of Science and Technology, Hirosaki University, 3 Bunkyo-Cho, Hirosaki, Aomori, 036-8561, Japan

[c] Division of Biological Science, Nara Institute of Science and Technology, 8916-5 Takayama, Ikoma, Nara 630-0192, Japan

*Corresponding authors: Sohei Yamada, so-yamada@bs.naist.jp, and Yoichiroh Hosokawa, hosokawa@ms.naist.jp

Author Contributions: S.Y. and Y.H. designed the research. N.I. supervised the research and contributed to presentation of the mechanism of axon outgrowth. S.Y. performed almost all experiments and data analysis. K.B. prepared primary cultured neurons. S.Y. and Y.H. wrote the article.

Keywords: Mechanobiology, Single cell manipulation, Laser application, Cell adhesion molecule, Actin

Abstract

Axon outgrowth is promoted by the mechanical coupling between the dynamic actin cytoskeleton and adhesive substrates via clutch and adhesion molecules in the axonal growth cone. In this study, we utilized a femtosecond laser-induced impulse to break the coupling between an axonal growth cone and an adhesive substrate, enabling us to evaluate the strength of the binding between proteins in the growth cone and a laminin substrate, and also determine the contribution of adhesion strength to axon outgrowth. We found that the adhesion strength of axonal L1 cell adhesion molecule (L1CAM)-laminin binding increased with the density of the laminin substrate. In addition, fluorescent speckle microscopy revealed that the retrograde flow of actin filaments in the axonal growth cone was dependent on the laminin density such that the flow speed reduced with increasing L1CAM-laminin binding. However, axon outgrowth did not increase monotonically with increased L1CAM-laminin binding but rather exhibited biphasic behavior, in which the outgrowth was suppressed by excessive L1CAM-laminin binding. Our quantitative evaluations of the adhesion strength suggest that the biphasic outgrowth is regulated by the balance between traction force and adhesion strength as a result of changes in the number of L1CAM-laminin interactions. These results imply that adhesion modulation is key to the regulation of axon guidance.

Significance Statement

There is a lack of a method to evaluate an adhesion strength of axonal growth cone. We evaluated the adhesion strength of axonal growth cones to a substrate by utilizing the force applied from a femtosecond laser impulse. This study shows that the adhesion strength between the growth cone and substrate is strengthened by L1CAM-laminin binding. Axon outgrowth did not increase monotonically with increased L1CAM-laminin binding but rather exhibited biphasic behavior, indicating that existence of suitable adhesion strength for axonal growth. Our findings suggest that the balance between growth cone adhesion strength and the traction force transmitted via cytoskeletal flow is a key factor in axon guidance.

Introduction

During neuronal development, axons elongate and form functional connections with other neurons and relevant cells. The growth cone located at the tip of an elongating axon senses chemical ligands in the external environment and undergoes directional migration (1-3). The traction force underlying growth cone migration is regulated by modulation of the coupling efficiency between actin filament (F-actin) retrograde flow and adhesive substrates via clutch and cell adhesion molecules (4, 5). Thus, the traction force transmitted to the substrate through the F-actin-adhesion coupling promotes axon outgrowth (1, 6).

We previously identified shootin1a and cortactin as clutch molecules for growth cone migration (7, 8). These molecules mediate the linkage between F-actin retrograde flow and the cytoplasmic domain of L1 cell adhesion molecule (L1CAM) (9). The extracellular domain of L1CAM interacts with adhesive ligands such as laminins in the extracellular matrix (10-12). L1CAM linked to the F-actin flow undergoes gripping (stop) and slipping (retrograde flow) on the substrate. It is the balance between these grip and slip states that regulates growth cone migration (12).

Our investigation focuses on the mechanism by which the interaction between L1CAM and laminin generates force. The challenge is to quantify key processes of growth cone migration, for which the adhesion strength via L1CAM-laminin binding is fundamental. However, it is difficult to quantify adhesion strength by conventional methods. For instance, the shear flow assay (13, 14) is not suitable for evaluating local adhesion at the interface between a growth cone and the substrate, whereas it is difficult to apply single-cell force spectroscopy (15, 16) to evaluate force without disturbing the adhesion required for axon outgrowth. We thus developed a method utilizing a femtosecond laser-induced impulsive force, which we used to quantify adhesions between leukocytes and endothelial cells, among epithelial cells, and between neurons and mast cells (17, 18). A near-infrared femtosecond laser focused through a lens objective into a water solution generates stress and shock waves at the laser focal point. These waves propagate out spherically and act as an impulsive force on nearby cells. The force is localized to a diameter of 1–10 μm and breaks intercellular adhesions at a single-cell resolution. We also developed a method to quantify the magnitude of the impulsive force by using atomic force microscopy (AFM) (19), enabling us to quantify the strength of intercellular adhesions on the basis of the force needed to break the connection (17, 18, 20).

In this work, we applied our previously established methods for generating laser-induced impulsive force (7, 12) to investigate the contribution of L1CAM-laminin binding to axon outgrowth. The specific interaction between laminin and L1CAM was confirmed by L1CAM knockdown in neurons. The strength of L1CAM-mediated adhesion was confirmed to be dependent on the density of laminin on the substrate. In addition, we used fluorescent speckle microscopy to observed the motions of F-actin and L1CAM in the axonal growth cone and then further assessed the contribution

of L1CAM-laminin binding to F-actin-substrate coupling. These experiments demonstrated that cytoskeletal dynamics in the axon growth cone are also dependent on the density of laminin on the substrate, revealing L1CAM-laminin binding as a mechanism for the regulation of axonal growth.

Results

Adhesion breaking by a femtosecond laser-induced impulsive force

Hippocampal neurons cultured for 3 days on a glass-bottom dish coated with 10 μg/ml laminin were placed on an inverted microscope equipped with a femtosecond laser irradiation system. The single-shot femtosecond laser pulses were focused in the vicinity of axonal growth cones to assess the adhesion breaking threshold (Fig. 1A). The force was estimated by measuring the distance from the growth cone at which the laser pulse broke the adhesion to the substrate. For example, the laser with a pulse energy of 700 nJ was initially focused at a position 20 μm from a targeted growth cone. After the first pulse irradiation, the focal point was moved closer to the target in 5 μm steps via an electrical stage until adhesion was broken; the distance between the growth cone and the final laser focal position was recorded.

Representative images before and after laser pulse irradiation are shown in Fig. 1B. The step-by-step approach of the laser pulse induces slight displacement of the growth cone (right image in Fig 1B; Video S1). This observation indicates that growth cones can be selectively detached from the substrate by the laser-induced impulsive force. We assessed whether the adhesion breaking process induced cell damage by using the fluorescent dye FM1-43 to mark sites of membrane repair (21). Significant increase in fluorescence did not occur when the laser was focused at the threshold distance for adhesion breaking (Fig. 1B), indicating that the impulsive force used to break growth cone adhesion does not damage the cell membrane.

Quantification of the adhesion breaking force

We evaluated the threshold distance (R) to break growth cone adhesion to the glass surface coated with 10 μg/ml laminin at different laser pulse energies (L) (Fig. 2A). As the impulsive force near the growth cone increases with L, the positive correlation between R and L indicates that R increases with an increasing impulsive force. We quantified the threshold for breaking the adhesion by using our previously established AFM method (22) in which an AFM cantilever replaces the tip of the growth cone and the impulsive force loaded on the cantilever is estimated from its bending

movement (17). From the estimation, the impulsive force F_0 generated at the laser focal point is related to L as follows:

$$F_0 = -0.003573L^2 + 0.644L - 1.5758. \quad [1]$$

Assuming that F_0 propagates spherically in the vicinity of the laser focal point, the impulsive force as a unit of pressure (P) is expressed by the following equation:

$$P\ (\mathrm{kPa}) = \frac{F_0\ (\mu\mathrm{N}) \times 10^3}{4\ \pi R^2\ (\mu m^2)}. \quad [2]$$

Figure 2B shows a histogram for pressures calculated with Eq. [2] for each data point in Fig. 2A; the distribution was almost Gaussian. The mean value of the minimum pressure to break growth cone adhesion to a 10 μg/ml laminin substrate was 4.5 kPa, comparable with the breaking threshold reported in our previous study (22).

Adhesion strength of the growth cone depends on L1CAM-laminin binding

Fluorescent dye-conjugated laminin was used to assess the density of laminin on the substrate (Fig. 2C). The intensity of fluorescence (I) increased with the concentration (C) of laminin used to coat the glass until reaching saturation (Fig. 2D). This relationship is described by the following equation:

$$I = I_{max}\left(1 - e^{-C/k}\right). \quad [3]$$

We assumed that (i) I is proportional to the number of laminin molecules attached to substrate N; (ii) N has a maximum that determines I_{max}; and (iii) the attachment rate k depends on the coating period (12 h in this experiment). In addition, we neglected the dissociation of laminin from the substrate because I was not significantly different after replacing the medium to one without laminin for the laser irradiation experiment. We defined the coverage rate (A) of laminin as an index of laminin density on the substrate using the following equation:

$$A = 1 - e^{-C/k}, \quad [4]$$

An A of 1 means that the laminin attached maximumly on the substrate. k was estimated by least-squares fitting with Eq. [3] and the data in Fig. 2D to obtain A on the substrate coated with laminin solution at concentration C.

The breaking threshold was evaluated according to A (red in Fig. 3) and compared with that determined after knockdown of L1CAM (blue in Fig. 3). The threshold increased with A for the control sample (Fig. 3B) but not for the L1CAM-knockdown samples, which maintained thresholds that matched those shown by controls at the low coverage rate (A = 0.01). These findings indicate that the adhesion strength between the growth cone and substrate is strengthened by L1CAM-laminin binding. The offset threshold (~2.5 kPa) likely reflects laminin-independent adhesive interactions.

The nearly linear increase in adhesion strength with increasing A in the control samples (Fig. 3B), despite the variability as a result of individual differences among the cells, suggests that

the adhesion strength due to the L1CAM-laminin binding is proportional to the laminin density on the substrate. Furthermore, as the adhesion strength is integral to the individual binding strength between L1CAM and laminin, the adhesion strength reflects the number of L1CAM-laminin interactions. Thus, the increase in the breaking threshold with *A* may reflect the increase in the number of the L1CAM-laminin interactions that occur with increased laminin density. This relationship is presumably satisfied until the L1CAM sites available for binding are saturated.

L1CAM-laminin binding promotes F-actin-adhesion coupling

The contribution of the laminin coverage rate *A* to F-actin-adhesion coupling was investigated next by visualizing F-actin retrograde flow and L1CAM molecules in filopodia at the growth cone. F-actin dynamics were observed by the motion of fluorescent actin speckles tagged with HaloTag (Fig. 4A ; Video S2; Video S3; Video S4) which were observed moving along filaments toward the leading edge of the growth cone. The speed at which they moved decreased linearly with increasing *A*, slowing from 3.70 μm/min at an *A* of 0.06 to 2.29 μm/min at an *A* of 0.99 (Fig. 4B). These data suggest that *A* promotes the cytoskeletal-adhesion coupling.

The dynamics of L1CAM-laminin binding were evaluated as grip and slip motions of L1CAM-HaloTag as shown in Fig. 4C (Video S5; Video S6; Video S7). The ratios of grip and slip states increased and decreased, respectively, with increasing *A* (Fig. 4D). Consistent with this, the speed at which HaloTag traveled (i.e., flow speed) decreased (Fig. 4E) while the duration spent in the grip phase increased (Fig. 4F) with increasing *A*. The differences between slip and grip states were proportionate to *A* in the range of 0.06 to 0.99.

L1CAM-laminin binding promotes the L1CAM grip state, transmitting the traction force to the substrate (12). With increased cytoskeletal-adhesion coupling, F-actin flow slows and the traction force transmitted to the substrate for growth cone migration increases (4, 23). Therefore, the linear associations described above support the result from the adhesion breaking test, i.e., the number of the L1CAM-laminin interactions, reflective of the adhesion strength of the growth cone, are nearly proportional to *A*. Conversely, the dissociation of L1CAM-laminin interactions disrupts cytoskeletal-adhesion coupling such that the force of retrograde flow is no longer transmitted to the substrate (12). The grip and slip motions observed in this study indicate that L1CAM-laminin binding is not static but changes dynamically. Thus, when the average number of L1CAM-laminin interactions between the growth cone and substrate is increased, the grip state is prolonged.

L1CAM-laminin binding results in biphasic axon outgrowth

Axon outgrowth also depends on *A*, as shown in Fig. 5. Axon lengths were the longest (>170 μm) when neurons were cultured under conditions where the laminin coverage rate (*A*) was between 0.45 and 0.78. However, the lengths of axons from L1CAM knockdown neurons were not affected

by *A* (blue bars in Fig. 5B), with shorter axons overall. These data suggest not only that axon outgrowth is regulated by L1CAM binding to the laminin substrate but also that this regulated outgrowth is biphasic.

Discussion

In an earlier study, we measured the traction force needed to translocate axonal growth cones on a laminin-coated substrate (8.2 ± 2.2 pN/μm^2) (12). The traction force is transmitted from F-actin retrograde flow; transmission is effective when the binding forces of the clutch and adhesion molecules between F-actin and substrate are higher than the traction force. The force to break the adhesion between the growth cone and substrate was on the order of kilopascals of pressure. Since the unit of force for traction (pN/μm^2) corresponds to pascals (Pa = N/m^2), the breaking force (>kPa) is >100 times stronger than the traction force in comparison with the average (~8 Pa). Thus, the adhesion between the growth cone and the substrate is strong enough to transmit the force of F-action retrograde flow to the substrate.

The number of L1CAM-laminin interactions is an important factor for transmitting the force of F-actin retrograde flow to the substrate. With few interactions, F-actin is not coupled to the adhesive substrate through clutch molecules (e.g., shootin1a and cortactin) and L1CAM. As a result, the force of retrograde flow is not effectively transmitted to the substrate to produce sufficient traction for axon outgrowth. This was demonstrated by the short axon lengths of neurons cultured on the substrate with low laminin density. By contrast, retrograde flow slows as the laminin density increases, indicating greater cytoskeletal-adhesion coupling that promotes transmission of the force from the flow to the traction force for growth cone migration. Our results indicate that laminin concentrations resulting in an *A* between 0.45 and 0.78 are optimal for providing suitable traction force.

Interestingly, we observed a decrease in axon growth at a high laminin density, suggesting that excessive L1CAM-laminin binding suppresses axon outgrowth. This biphasic behavior was also reported for integrin-ligand binding (24-26). Those studies investigated the migration of fibroblast and muscle cells when using various concentrations of substrate ligands, integrin expression levels, and integrin-ligand binding affinities. Cell adhesion strength was evaluated by share-stress flow assay and compared with the migration speed. With strong adhesion, the cells spread and extended lamellae, but the cell body did not move. The suppression of migration was attributed to the inability of cells to overcome adhesion to the substrate (26-28). For axons, outgrowth is promoted not only by the traction force at the forward side but also by detachment of the back side. Thus, the decrease in growth we observed may be attributable to a lack of detachment as a result of excessive L1CAM-laminin interactions. The cytoskeletal-adhesion coupling that generates traction force is enhanced with increasing *A*; thus the balance between the

traction force with the cytoskeletal-adhesion coupling and growth cone adhesion is key for regulating the axon guidance.

Notably, axon outgrowth was suppressed when *A* increased from 0.78 to 0.99, an estimated proportional increase in adhesion strength of ~20%. This result indicates that the modification of outgrowth is on the order of 10% of the modification in the adhesion strength as a result of the number of L1CAM-laminin interactions. Our data therefore suggest that these interactions are responsible for adhesion to the substrate and thus for the regulation of axon guidance. This regulation is key for growth cone migration and axon outgrowth through the extracellular matrix in brain, thereby contributing to the formation of network connections with other neurons and relevant cells.

Conclusion

This investigation utilized femtosecond laser impulses to quantitatively evaluate the adhesion strength between axonal growth cones and a laminin substrate. The data show that the strength of the L1CAM-laminin interactions increases with the laminin density. Notably, axon outgrowth does not increase monotonically with increased L1CAM-laminin binding but instead exhibits biphasic behavior, in which outgrowth is suppressed in the presence of high amounts of L1CAM-laminin binding. This biphasic outgrowth is regulated by altered adhesion caused by changes in the number of binding interactions on the order of 10%. These results suggest that the balance between the traction force from the cytoskeletal-adhesion coupling and growth cone adhesion is one of the keys to regulating axon guidance. Future studies on the biphasic regulation of axon outgrowth should seek to further elucidate the guidance mechanism.

Materials and Methods

Preparation of cell culture substrate

For each experiment, a 35 mm glass-bottom dish (Matsunami, Osaka, Japan) was coated with 100 μg/ml poly-lysine (FUJIFILM WAKO Pure Chemical Corporation) at 37°C for 12 h. After washing, the plate was coated with laminin (laminin 1; FUJIFILM WAKO Pure Chemical Corporation) in phosphate-buffered saline (PBS) at 37°C for 12 h. The surfaces were washed three times with PBS. The laminin density on the dish was modified by altering the concentration of the deposited laminin solution (0.01–100 μg/ml). The laminin density was evaluated by coating the dish with laminin conjugated to a fluorescent dye (green fluorescent HiLyte 488; Cytoskeleton), which was observed under a confocal laser scanning microscope (Zeiss LSM710; excitation, 488 nm; emission, 510 nm). The fluorescence intensity was estimated as an area integration (15 × 15 μm) of the substrate fluorescence.

Cell culture

Hippocampal neurons were prepared from embryonic day 18 rats and seeded on glass-bottom dishes. To induce axon outgrowth, neurons were cultured in neurobasal medium (Thermo Fisher Scientific) containing B-27 supplement (Thermo Fisher Scientific) and 1 mM glutamine for 3 days. All relevant aspects of the experimental procedures were approved by the Institutional Animal Care and Use Committee of Nara Institute of Science and Technology.

Femtosecond laser irradiation system

The cultures were imaged on an inverted microscope (IX71; Olympus) utilizing femtosecond laser pulses from a regeneratively amplified Ti:Sapphire femtosecond laser (800 ± 5 nm, 100 fs, <1 mJ/pulse, 32 Hz) (Solstice Ace; Spectra-Physics). The pulse was focused near the growth cone (Fig. 1A) through a 100× lens objective (UMPlanFI, numerical aperture [NA], 1.25; Olympus). The irradiation was controlled by a mechanical optical shutter (Σ-65GR; Sigma Koki). The laser pulse energy was tuned by a half-wave (λ/2) plate and dual polarizers. A single femtosecond pulse (50–1,000 nJ/pulse) was applied near the growth cone, and adhesion breaking was monitored by a charge-coupled-device (CCD) camera.

Evaluation of cell damage by FM1-43 dye

A cell-impermeant lipophilic dye (FM1-43; Thermo Fisher Scientific) was used to evaluate cell damage induced by the adhesion breaking process. The fluorescent dye is incorporated into inner membrane lipids after a cell membrane breaks. The dye was added to the culture medium at a

concentration of 2.5 mM 30 min before the laser irradiation and was then visualized using a confocal laser scanning microscope system (excitation: 473 nm, emission: 580 nm, FV300; Olympus) coupled to the inverted microscope used for laser irradiation experiments.

Impulsive force measurement system using AFM

AFM was used to quantify the force needed to break the adhesion, as described previously (17). An AFM cantilever (thickness, 4.0 μm; length, 125 μm; width, 30 μm; force constant, 42 N/m; resonance frequency, 330 Hz in air) (TL-NCH-10; Nano World, Neuchatel, Switzerland) was attached to the AFM head (Nano Wizard 4 BioScience; JPK Instruments, Berlin, Germany) and placed in pure water on the microscope stage. The laser pulse was focused 10 μm away from the top of the cantilever. The transient oscillation of the cantilever induced by the laser pulse irradiation was detected by an oscilloscope. The magnitude of the cantilever movement was estimated from the oscillation.

L1CAM knockdown experiment

L1CAM knockdown neurons were prepared by using a Block-iT Pol II miR RNAi expression kit (Invitrogen). The targeting sequence of L1CAM miRNA #1, 5′-GTGGAGGAAGGAGAATCAGTA-3′, corresponds to nucleotides 439 to 459 in the coding region of rat L1CAM was reported previously (12). Hippocampal neurons were transfected with the miRNA expression vector and incubated for 20 h. The cells were then collected and cultured on the laminin-coated glass-bottom dishes. In this system, GFP is expressed with the L1CAM miRNA, enabling the growth cones of transfected cells to be visualized and monitored.

Fluorescent speckle microscopy

The retrograde flow of F-actin and slip and grip motions of L1CAM were investigated by fluorescent speckle microscopy. HaloTag-actin and L1CAM-HaloTag were expressed in hippocampal neurons. To introduce HaloTag tetramethylrhodamine (TMR) to L1CAM-HaloTag and HaloTag-actin, hippocampal neurons were incubated with HaloTag TMR ligand (Promega) at a 1:1,500 dilution in L15 medium containing B27 supplement and 1 mM glutamine for 1 h at 37°C. The medium was then replaced with fresh L15 medium. The preparation method of HaloTag-actin is specified in the literature (12).

HaloTag-actin speckles were observed at 37°C using a fluorescence inverted microscope (Axio Observer A1; Carl Zeiss) equipped with a C-apochromat 63× NA 1.20 lens objective (Carl Zeiss), an illumination laser (561 nm), and an EM-CCD camera (Ixon3; Andor). Fluorescent L1CAM-HaloTag speckles in growth cones were observed using total internal reflection fluorescence (TIRF) on an inverted microscope (IX81; Olympus) equipped with a TIRF lens

objective (UAPON 100×OTIRF NA 1.49; Olympus), an illumination laser (488 nm), and a scientific complementary metal-oxide semiconductor (sCMOS) camera (ORCA Flash4.0LT; HAMAMATSU). The flow speed of F-actin and slip speed of L1CAM were analyzed by monitoring the fluorescence signals of the HaloTags at 5 s intervals. L1CAM puncta that were visible for at least 10 s (two intervals) were analyzed; immobile ones were defined as L1CAM in stop (grip) phase, while those that flowed retrogradely were defined as in flow (slip) phase.

Evaluation of neurite length by immunofluorescence staining

Axon length was evaluated by immunofluorescence imaging. Neurons were cultured for 3 days on the laminin-coated dishes, fixed with 3.7% formaldehyde in PBS overnight at 4°C, treated for 15 min with 0.05% Triton X-100 in PBS at 4°C, and then incubated with 10% fetal bovine serum in PBS overnight at 4°C. The cells were then incubated with an anti-GFP antibody (Invitrogen), as described by Toriyama et al. (24), and observed with a confocal laser scanning microscope (excitation, 488 nm; emission, 510 nm; LSM 710). The lengths of all axons of 50 cells were measured for each coverage rate.

Statistical analysis

Differences in means were analyzed by the paired t-test. The results of the t-test were considered significant when $P < 0.05$.

Acknowledgments

We thank Dr. Ryohei Yasukuni and Dr. Kazunori Okano (Nara Institute of Science and Technology, Japan) for fruitful discussions.

Funding

This research was supported in part by AMED under grant number 21gm0810011h0005, ACT-X under grant number JPMJAX191K, and the Foundation of Nara Institute of Science and Technology.

References

1. A. L. Kolodkin, M. Tessier-Lavigne, Mechanisms and molecules of neuronal wiring: a primer. Cold Spring Harb Perspect Biol 3 (2011).

2. L. A. Lowery, D. Van Vactor, The trip of the tip: understanding the growth cone machinery. Nat Rev Mol Cell Biol 10, 332-343 (2009).

3. K. Franze, Integrating Chemistry and Mechanics: The Forces Driving Axon Growth. Annu Rev Cell Dev Biol 36, 61-83 (2020).

4. D. M. Suter, P. Forscher, Substrate-cytoskeletal coupling as a mechanism for the regulation of growth cone motility and guidance. J Neurobiol 44, 97-113 (2000).

5. N. A. Medeiros, D. T. Burnette, P. Forscher, Myosin II functions in actin-bundle turnover in neuronal growth cones. Nat Cell Biol 8, 215-226 (2006).

6. C. E. Chan, D. J. Odde, Traction dynamics of filopodia on compliant substrates. Science 322, 1687-1691 (2008).

7. T. Shimada et al., Shootin1 interacts with actin retrograde flow and L1-CAM to promote axon outgrowth. J Cell Biol 181, 817-829 (2008).

8. Y. Kubo et al., Shootin1-cortactin interaction mediates signal-force transduction for axon outgrowth. J Cell Biol 210, 663-676 (2015).

9. K. Baba et al., Gradient-reading and mechano-effector machinery for netrin-1-induced axon guidance. Elife 7 (2018).

10. H. Hall, S. Carbonetto, M. Schachner, L1/HNK-1 carbohydrate- and beta 1 integrin-dependent neural cell adhesion to laminin-1. J Neurochem 68, 544-553 (1997).

11. T. Esch, V. Lemmon, G. Banker, Local presentation of substrate molecules directs axon specification by cultured hippocampal neurons. Journal of Neuroscience 19, 6417-6426 (1999).

12. K. Abe et al., Grip and slip of L1-CAM on adhesive substrates direct growth cone haptotaxis. Proceedings of the National Academy of Sciences of the United States of America 115, 2764-2769 (2018).

13. S. Gupton, C. Waterman-Storer, Spatiotemporal feedback between actomyosin and focal-adhesion systems optimizes rapid cell migration. Cell 125, 1361-1374 (2006).

14. J. de Rooij, A. Kerstens, G. Danuser, M. Schwartz, C. Waterman-Storer, Integrin-dependent actomyosin contraction regulates epithelial cell scattering. Journal of Cell Biology 171, 153-164 (2005).

15. M. Benoit, D. Gabriel, G. Gerisch, H. Gaub, Discrete interactions in cell adhesion measured by single-molecule force spectroscopy. Nature Cell Biology 2, 313-317 (2000).

16. M. Krieg et al., Tensile forces govern germ-layer organization in zebrafish. Nature Cell Biology 10, 429-U122 (2008).

17. Y. Hosokawa, Applications of the femtosecond laser-induced impulse to cell research. Japanese Journal of Applied Physics 58 (2019).

18. Y. Hosokawa, M. Hagiyama, T. Iino, Y. Murakami, A. Ito, Noncontact estimation of intercellular breaking force using a femtosecond laser impulse quantified by atomic force microscopy. Proceedings of the National Academy of Sciences of the United States of America 108, 1777-1782 (2011).

19. T. Iino, M. Hagiyama, T. Furuno, A. Ito, Y. Hosokawa, Time-Course Statistical Evaluation of Intercellular Adhesion Maturation by Femtosecond Laser Impulse. Biophysical Journal 111, 2255-2262 (2016).

20. K. Oikawa et al., Physical interaction between peroxisomes and chloroplasts elucidated by in situ laser analysis. Nat Plants 1, 15035 (2015).

21. C. Cai et al., MG53 nucleates assembly of cell membrane repair machinery. Nature Cell Biology 11, 56-U108 (2009).

22. S. Yamada, T. Iino, Y. Bessho, Y. Hosokawa, T. Matsui, Quantitative analysis of mechanical force required for cell extrusion in zebrafish embryonic epithelia. Biology Open 6, 1575-1580 (2017).

23. M. Toriyama et al., Shootin1: a protein involved in the organization of an asymmetric signal for neuronal polarization. Journal of Cell Biology 175, 147-157 (2006).

24. S. Palecek, J. Loftus, M. Ginsberg, D. Lauffenburger, A. Horwitz, Integrin-ligand binding properties govern cell migration speed through cell-substratum adhesiveness. Nature 385, 537-540 (1997).

25. DiMilla PA, Barbee K, Lauffenburger DA. Mathematical model for the effects of adhesion and mechanics on cell migration speed. Biophysical Journal 60, 15-37 (1991).

26. A. Huttenlocher, M. H. Ginsberg, A. F. Horwitz, Modulation of cell migration by integrin-mediated cytoskeletal linkages and ligand-binding affinity. J Cell Biol 134, 1551-1562 (1996).

27. M. P. Sheetz, D. P. Felsenfeld, C. G. Galbraith, Cell migration: regulation of force on extracellular-matrix-integrin complexes. Trends Cell Biol 8, 51-54 (1998).

28. T. Minegishi, N. Inagaki, Forces to Drive Neuronal Migration Steps. Front Cell Dev Biol 8, 863 (2020).

29. K. Hennig et al., Stick-slip dynamics of cell adhesion triggers spontaneous symmetry breaking and directional migration of mesenchymal cells on one-dimensional lines. Sci Adv 6, eaau5670 (2020).

444 **Figures**

445

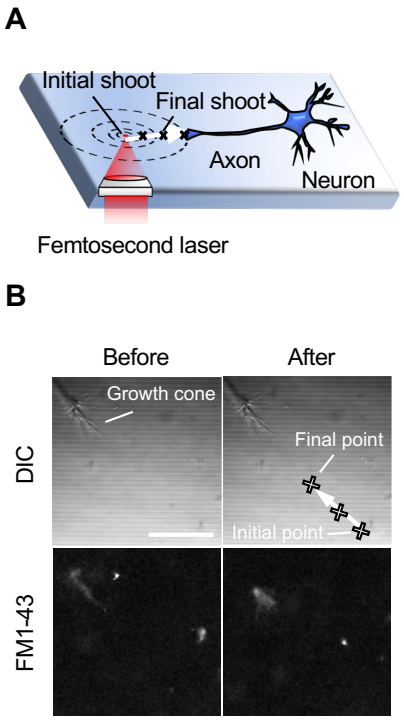

446

447 **Figure 1. Observation of adhesion breaking of an axonal growth cone by femtosecond laser-**
448 **induced impulsive force.** (A) Schematic of the spatial relation between the femtosecond laser
449 pulse and targeted axonal growth cone of a neuron cultured in a dish coated with 10 μg/ml laminin.
450 The laser focal point was sequentially moved closer to the growth cone, as indicated by an arrow.
451 (B) Representative results of adhesion breaking of a growth cone. Top and bottom panels are
452 differential interference contrast (DIC) and fluorescence images before (left) and after (right) the
453 final pulse irradiation, which induces the detachment of the growth cone. Before the final irradiation,
454 the pulse was sequentially focused closer to the growth cone, indicated as cross points (laser focal
455 point) on the arrowed line in the top right image. The white silhouettes in the bottom fluorescence
456 microphotographs are weak fluorescence from FM1-43 dye used to evaluate damage of the growth
457 cone. Scale bar, 10 μm.

458

459

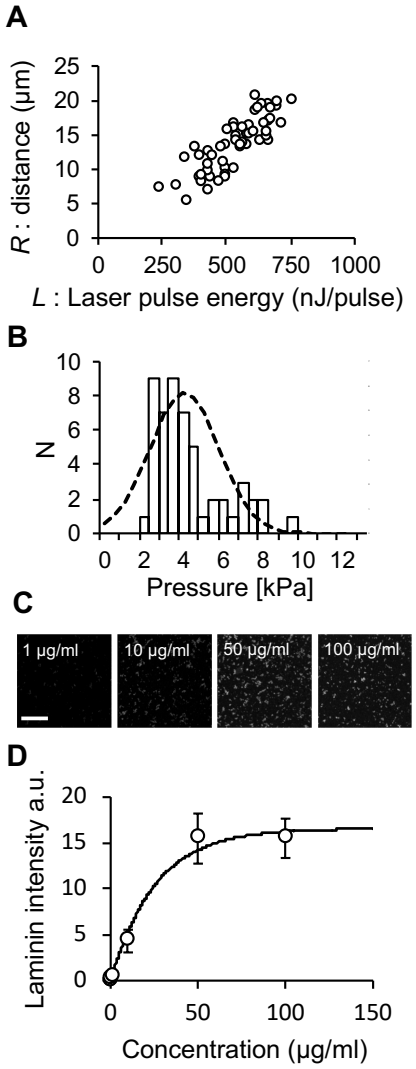

Figure 2. Quantitative evaluation of breaking force for growth cone adhesion by using femtosecond laser impulsive force. (A) Pulse energy *L* dependence of threshold distance *R* to break the growth cone adhesion on a glass substrate coated with a 10 μg/ml laminin solution, corresponding to an *A* of 0.45 (see Eq. [4]). *n* = 36. (B) Histogram of the adhesion breaking threshold. The vertical axis *N* is number of cells. The threshold was calculated independently by substituting data from panel A into Eq. [2]. (C) Images of fluorescent dye-conjugated laminin on the substrate. Concentrations of the laminin solution used for the coating are indicated at the top. Scale bar, 10 μm. (D) Fluorescence intensity as a function of the laminin concentration. The fluorescence intensities were measured on substrates coated with laminin solutions with concentrations of 0.01,

472 0.1, 1, 10, 50, and 100 μg/ml. The fitting curve was calculated by Eq. [3], where I_{max} = 25.5 and k =
473 16.6. n = 50 for each concentration. Data are means ± SDs from three independent experiments.
474

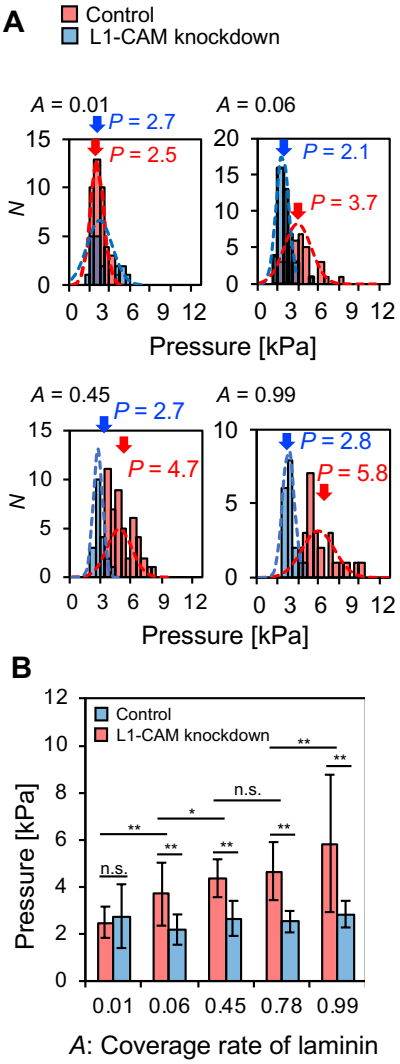

Figure 3. Adhesion breaking of growth cone on a laminin-coated substrate.

(A) Representative results of the adhesion breaking threshold. The coverage rate of laminin (*A*) is indicated at the top. The vertical axis *N* is number of cells. Red and blue histograms are for control neurons and L1CAM knockdown neurons. (B) Means and SDs of the breaking threshold. Control neurons: n = 41, 35, 36, 12, and 25 signals for A = 0.01, 0.06, 0.45, 0.78, and 0.99, respectively. L1CAM knockdown neurons: n = 18, 44, 34, 20, and 19 signals for A = 0.01, 0.06, 0.45, 0.78, and 0.99, respectively. *p < 0.05, **p < 0.01 (two-tailed Student's t test), n.s., not significant.

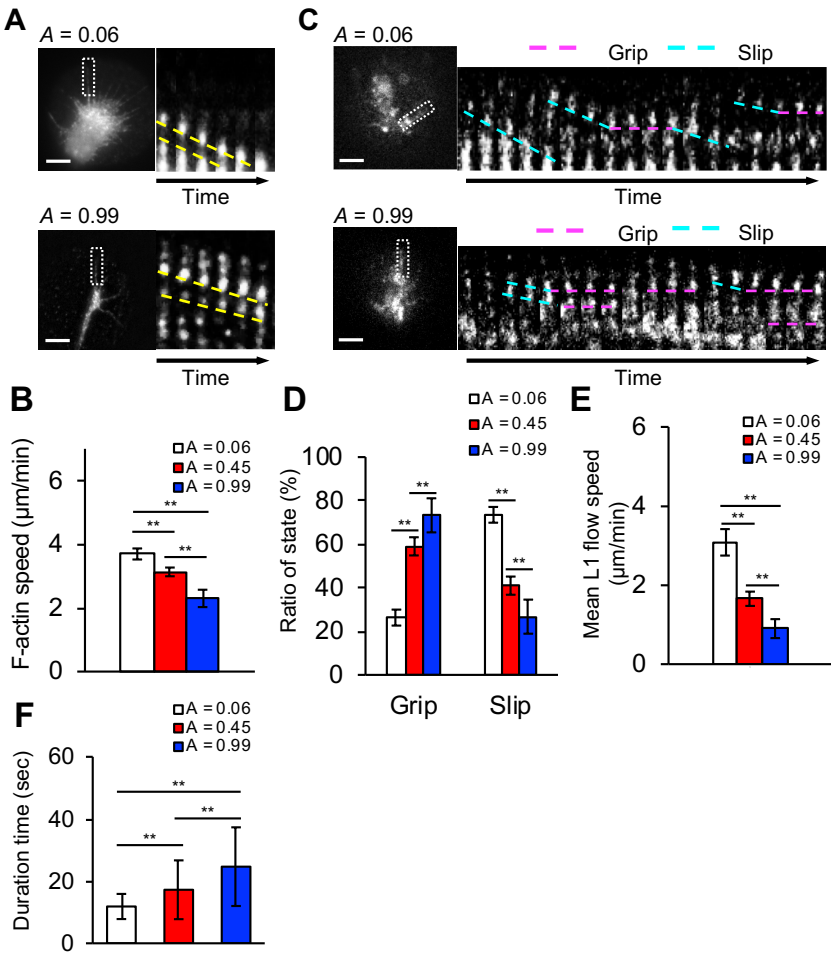

Figure 4. Molecular dynamics of F-actin and L1CAM in the axonal growth cone detected by fluorescence speckle microscopy. (A) Fluorescence speckle images of the HaloTag-actin in a filopodium extended from an axonal growth cone. The coverage rate of laminin (*A*) is indicated at the top. Kymographs (right) depict HaloTag-actin behavior in boxed region in the image on the left. Slope of the yellow dashed line corresponds to retrograde flow speed of the F-actin. Time interval between frames, 5 s. Scale bar, 5 μm. (B) Retrograde flow speed of F-actin. *n* = 125, 160, and 130 signals for *A* = 0.06, 0.45, and 0.99, respectively. (C) Fluorescence speckle images of L1CAM-HaloTag in a filopodium. Kymographs (right) depict L1CAM-HaloTag behavior in a boxed region in the image on the left. Dashed pink and blue lines connect L1CAM in grip and slip states, respectively. Time interval between frames, 5 s. Scale bar, 5 μm. Ratios (D) and flow speeds (E) of the grip and slip states of L1CAM-HaloTag in filopodia obtained from the kymograph analyses. *n* = 261, 450, and 197 signals for *A* = 0.06, 0.45, and 0.99, respectively. (E) Flow speed of L1CAM-HaloTag in the slip state. The speed corresponds to slopes of dashed blue lines in panel C. (F)

Durations of L1-HaloTag grip. White, red, and blue bars represent data for A = 0.06, 0.45, and 0.99, respectively. Data are means ± SDs; $^{**}p < 0.01$.

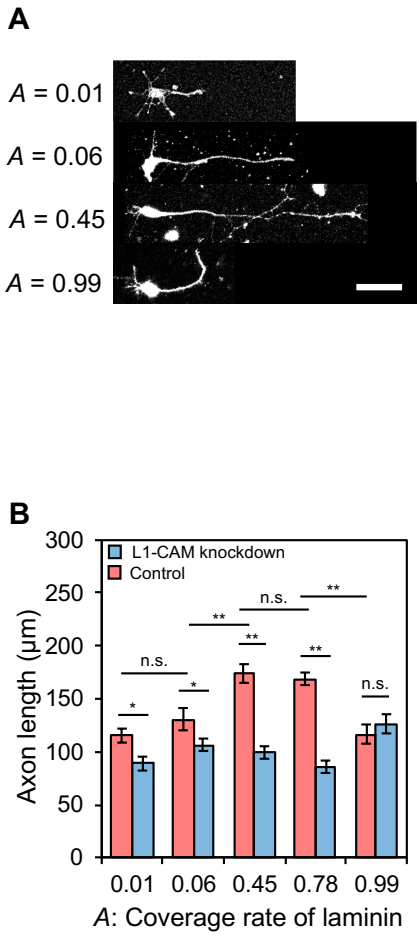

Figure 5. **Elongation of neurites on laminin-coated substrate.**

(A) Confocal images of neurons visualized with a GFP antibody. The coverage rate of laminin (*A*) is indicated on the left. Scale bar, 100 μm. (B) Mean values and SDs of axon length. Control neurons: n = 91, 28, 79, 60, and 71 signals for A = 0.01, 0.06, 0.45, 0.78, and 0.99, respectively; L1CAM knockdown neurons: n = 43, 49, 73, 103, and 48 signals for A = 0.01, 0.06, 0.45, 0.78, and 0.99, respectively. *p < 0.05, **p < 0.01. n.s., not significant.